Lattice thermal transport in La_{3}Cu_{3}X_{4} compounds (X=P,As,Sb,Bi): Interplay of anharmonicity and scattering phase space

Tribhuwan Pandey, Carlos A. Polanco, Lucas Lindsay, and David S. Parker

Phys. Rev. B **95**, 224306 — Published 30 June 2017

DOI: 10.1103/PhysRevB.95.224306

Lattice thermal transport in $La_3Cu_3X_4$ (X = P, As, Sb, Bi) compounds: Interplay of anharmonicity and scattering phase space

Tribhuwan Pandey, Carlos A. Polanco, Lucas Lindsay, and David S. Parker
Materials Science and Technology Division,
Oak Ridge National Laboratory, Oak Ridge, Tennessee 37831, USA
(Dated: June 5, 2017)

Abstract

Thermal conductivity of $La_3Cu_3X_4$ (X=P, As, Sb, Bi) compounds are examined using first-principles density functional theory and Boltzmann transport methods. We observe a trend of increasing lattice thermal conductivity (κ_l) with increasing atomic mass, challenging our expectations as lighter mass systems typically have larger sound speeds and weaker intrinsic scattering. In particular, we find that $La_3Cu_3P_4$ has the lowest κ_l despite having larger sound speed and the most restricted available phase space for phonon-phonon scattering, an important criterion for estimating and comparing κ_l among like systems. The origin of this unusual behavior lies in the strength of the individual anharmonic phonon scattering matrix elements, which are much larger in $La_3Cu_3P_4$ than in the heavier $La_3Cu_3Bi_4$ system. Our finding provides insights into the interplay of harmonic and anharmonic properties of complex, low thermal conductivity compounds, of potential use for thermoelectric and thermal barrier coating applications.

I. INTRODUCTION

At the heart of efficient thermoelectric device design lies the identification and manipulation of a material with low lattice thermal conductivity (κ_l), large thermopower and high electrical conductivity [1-3]. Generally low κ_l is observed in compounds composed of heavy elements with complicated crystal structures[4,5]. In this regard the rare earth based homologous compounds $La_3Cu_3X_4$ (X = P, As, Sb Bi) with large and complex unit cells (40 atoms) may be a promising class of materials for such applications. Among these $La_3Cu_3Sb_4$ and $La_3Cu_3Bi_4$ are experimentally known [6-9], and $La_3Cu_3Sb_4$ has been described as a degenerate *p*-type semiconductor with high electrical conductivity, moderate thermopower ($\sim$150 $\mu V/K$), and κ_l of 2.5 W/m-K at room temperature [6-9]. $La_3Cu_3P_4$ and $La_3Cu_3As_4$ have not been realized experimentally, however, our recent work [10] in crystal structure prediction and thermodynamic stability analysis demonstrates that these are likely to be formed in the space group *I-43d,* same as $La_3Cu_3Sb_4$ and $La_3Cu_3Bi_4$.

Even in isoelectronic, homologous compounds interesting variations in the landscape of κ_l can be obtained simply from variance of the masses of the constituent elements, as these are a key feature in determining vibrational properties. Variation of constituent element masses alters the phonon dispersion and thereby the group velocities. Also it changes the phonon lifetimes via modulation of available scattering due to energy and momentum conservation conditions. Thus mass variance can be an effective tool to manipulate κ_l, and has been employed to engineer thermal transport in a variety of thermoelectric materials [1,11-14]. Here, we use a first principles phonon Boltzmann equation (PBE) method to examine and compare vibrational properties and κ_l of $La_3Cu_3P_4$, $La_3Cu_3As_4$, $La_3Cu_3Sb_4$ and $La_3Cu_3Bi_4$.

Despite having the smallest average mass $La_3Cu_3P_4$ exhibits the lowest κ_l of this series of compounds. The origin of this atypical behavior is rooted in the complex interplay of vibrational features: atomic masses, phonon velocities, scattering phase space and anharmonicity, components that determine κ_l. Often these are examined individually to understand the dominant properties governing transport. However, considering each factor individually in the $La_3Cu_3X_4$ systems does not give a clear picture of the conductivity trends, in fact comparing individual trends leads to contradictory findings. In particular, we find an unusual interplay of individual scattering matrix elements and overall scattering phase space giving strongly opposite trends in determining κ_l of these systems, the latter increasing κ_l and the former decreasing κ_l in going from $La_3Cu_3P_4$ to $La_3Cu_3Bi_4$.

Here we provide quantitative, physical insights into the correlation of vibrational properties that determine κ_l of the $La_3Cu_3X_4$ systems to provide a more fundamental understanding of lattice transport in these and other complex unit cell materials, elucidating avenues for engineering thermal transport in large unit cell systems. Section II briefly discusses the theoretical methods employed. Section III presents thermal conductivity results and discussion of these related to basic vibrational properties. Section IV provides a summary of this work.

II. THEORETICAL METHODS

The lattice thermal conductivities were calculated by solving the PBE using an iterative method [15] with interatomic forces from density functional theory (DFT). For the cubic systems considered here κ_l is a scalar quantity given by:

$$\kappa_l = \kappa_l^{\alpha\alpha} = \frac{1}{NV}\sum_\lambda C_\lambda v_\lambda^\alpha v_\lambda^\alpha \tau_\lambda^\alpha \qquad (1)$$

where λ denotes a phonon mode in branch p with wavevector $\boldsymbol{q}$, v_λ is the phonon group velocity, C_λ is the specific heat, τ_λ is the lifetime with an applied temperature gradient in the α^{th} direction, N is the number of $\boldsymbol{q}$ points uniformly sampled in the Brillouin zone, and V is the volume of the unit cell. $1/\tau_\lambda$ is given by the sum of all possible transition probabilities for mode λ with modes λ' and λ'' [16]:

$$\Gamma^{\pm}_{\lambda\lambda'\lambda''} = \frac{\hbar}{8N_0}\begin{Bmatrix} n^0_{\lambda'} - n^0_{\lambda''} \\ n^0_{\lambda'} + n^0_{\lambda''} + 1 \end{Bmatrix} |\Phi_{\lambda\lambda'\lambda''}|^2 \frac{\delta(\omega_\lambda \pm \omega_{\lambda'} - \omega_{\lambda''})}{\omega_\lambda \omega_{\lambda'} \omega_{\lambda''}} \qquad (2)$$

that satisfy momentum and energy conversation [17]. N_0 is the number of unit cells in the crystal; ω_λ is the angular frequency corresponding to the λ^{th} mode, the $\pm$ corresponds to phonon absorption and emission processes, and $|\Phi_{\lambda\lambda'\lambda''}|^2$ are the scattering matrix elements given by:

$$\Phi_{\lambda\lambda'\lambda''} = \sum_k \sum_{l'k'} \sum_{l''k''} \sum_{\alpha\beta\gamma} \Phi_{\alpha\beta\gamma}(0k, l'k', l''k'') \frac{e^\lambda_{\alpha k} e^{\lambda'}_{\beta k'} e^{\lambda''}_{\gamma k''}}{\sqrt{M_k M_{k'} M_{k''}}} e^{i\boldsymbol{q}'\cdot\boldsymbol{R}_{l'}} e^{i\boldsymbol{q}''\cdot\boldsymbol{R}_{l''}} \qquad (3)$$

with e^α_λ the α^{th} component of an eigenvector, M_k the atomic mass of the k^{th} atom, and $\Phi_{\alpha\beta\gamma}(0k, l'k', l''k'')$ the anharmonic IFCs. Diagonalization of the dynamical matrix gives the phonon frequencies ω_λ and eigenvectors.

Harmonic IFCs, were obtained using the finite displacement method with the

Phonopy [18,19] package using 2×2×2 supercells and 3×3×3 **k**-point grids. The effect of supercell sizes on the phonon frequencies was investigated by using 2×2×2 (160 atoms), and 3×3×3 (540 atoms) supercells for $La_3Cu_3Bi_4$. The phonon dispersion was found to be nearly identical for both the cases, ensuring well converged phonon frequencies for 2×2×2 supercell. Anharmonic IFCs were calculated using 2×2×2 supercells and Γ-point only calculations. Interactions were considered out to third-nearest neighbors of the unit cell atoms for anharmonic IFCs. DFT calculations employed the projector augmented wave (PAW) method [20] as implemented in the Vienna ab initio simulation package (VASP) [20-22] with the generalized gradient approximation according to Perdew, Burke, and Ernzerhof [23]. Eleven valence electrons for La ($5s^2 5p^6 5d^1 6s^2$), 11 for Cu ($3d^{10} 4s^1$), 5 for P ($3s^2 3p^3$), 5 for As ($4s^2 4p^3$), 5 for Sb ($5s^2 5p^3$), and 5 for Bi ($6s^2 6p^3$) were used in the PAW potentials. For accurate phonon frequencies, a high energy cutoff of 600 eV and strict energy convergence criterion of 10^{-8} eV were used. The ShengBTE [24-26] package was employed to iteratively solve the PBE. Within ShengBTE a Gaussian function is used to approximate the Dirac delta distribution which arises from the conservation of energy for each scattering process. The convergence of room temperature κ_l as function of **q**-point integration grid at various Gaussian widths (marked as SB) is shown in Appendix **Figure 10** for $La_3Cu_3P_4$ and $La_3Cu_3Bi_4$. The remaining two systems exhibit similar convergence behavior. For well converged κ_l values, a **q**-grid of 25×25×25 and a Gaussian smearing parameter of 0.5 was used. All calculations are performed using fully relaxed crystal structures with optimized lattice parameters. Relaxed crystal structures and calculated IFCs can be found in Supplementary Material [27].

III. RESULTS AND DISCUSSION

Figure 1(a) gives calculated κ_l versus temperature for $La_3Cu_3P_4$ (pink diamonds), $La_3Cu_3As_4$ (green circles), $La_3Cu_3Sb_4$ (red squares) and $La_3Cu_3Bi_4$ (blue triangles). Each material demonstrates the typical κ_l~1/T behavior, characteristic of intrinsic three-phonon scattering resistance. We find that phonon-isotope scattering [28,29] is insignificant in all systems for the temperatures considered 100K<T<1000K, at most reducing κ_l by 2% at 100K. For example κ_l of isotopically pure (natural) $La_3Cu_3Sb_4$ is found to be 8.67 W/m-K (8.50 W/m-K) at 100 K and 2.6 W/m-K (2.58 W/m-K) at 300 K. Measured data for κ_l is only available for polycrystalline $La_3Cu_3Sb_4$ [7] and is given by black ×'s. Calculated and measured κ_l values seem to approach each other at the highest measured temperatures. However, the measured κ_l versus T behavior does not give the typical trend dictated by Umklapp resistance and the κ_l values at the lowest temperatures are significantly suppressed. Likely extrinsic scattering

mechanisms such as grain boundaries present in polycrystalline samples are causing this discrepancy and the nearly flat temperature behavior of κ_l.

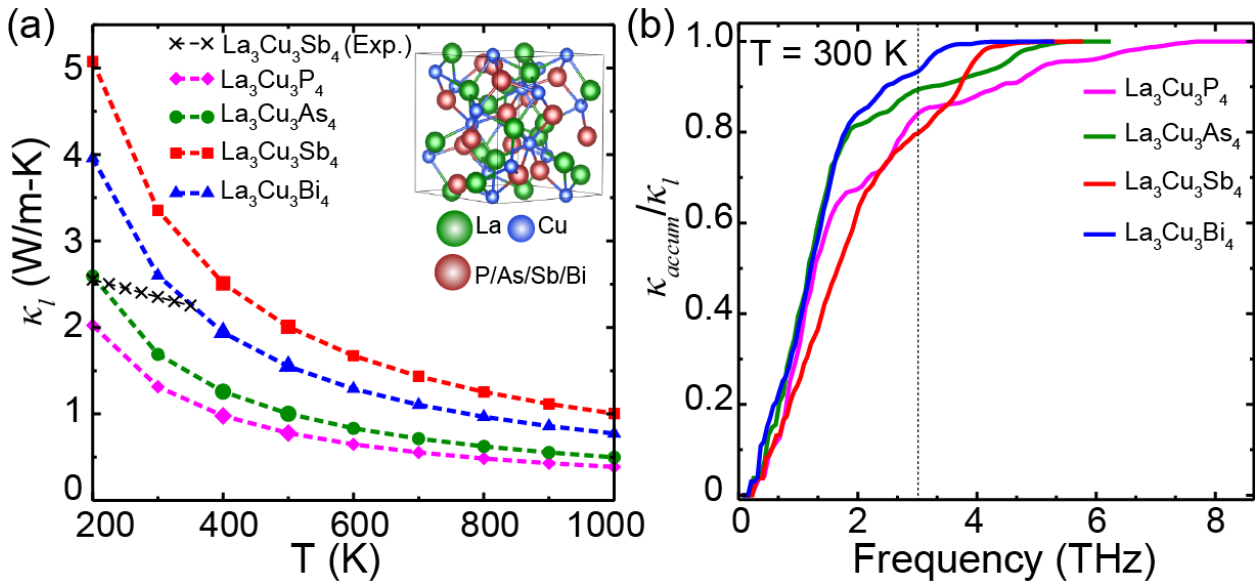

Figure 1. (a) Calculated κ_l versus temperature for $La_3Cu_3P_4$ (pink diamonds), $La_3Cu_3As_4$ (green circles), $La_3Cu_3Sb_4$ (red squares) and $La_3Cu_3Bi_4$ (blue triangles). Measured κ_l values (black ×'s) are given for $La_3Cu_3Sb_4$ [7]. (b) Cumulative thermal conductivity scaled by the total κ_l for each system as a function of frequency at 300K. The inset in (a) represents the crystal structure of these compounds.

Over the entire temperature range, κ_l is minimum for the lightest material, $La_3Cu_3P_4$, followed by $La_3Cu_3As_4$, $La_3Cu_3Bi_4$ and $La_3Cu_3Sb_4$ in increasing order of conductivity. In particular, we find κ_l of $La_3Cu_3P_4$ is 1.31 W/m-K at 300 K, similar to that of the prototypical thermoelectric material Bi_2Te_3 [30,31] and nearly 2.5 times lower than that of heavier $La_3Cu_3Bi_4$. This is surprising as it is expected that lower mass materials should have larger κ_l. Based partly on the work of Leibfried and Schlömann [32], and in the context of high κ_l materials, Slack outlined four crystal properties that govern κ_l [4,33]: (i) average atomic mass, (ii) interatomic bonding (iii) crystal structure and (iv) anharmonicity. More specifically, large mass materials with weak bonding have lower frequency phonons, thus lower velocity heat carriers. This is often characterized by the Debye temperature Θ_D (defined in the Appendix) which gives a measure of properties (i) and (ii) and is correlated with C_λ and v_λ in **Eq. 1.** M_{avg} and Θ_D for the $La_3Cu_3X_4$ are given in **Table I** along with the Debye velocity $v_{D^{-3}} = \frac{2}{3}v_{TA}^{-3} + \frac{1}{3}v_{LA}^{-3}$, which gives a measure of the sound speed of these systems. v_{LA} and v_{TA}

are the longitudinal (LA) and transverse (TA) acoustic velocities near the zone center along the $\Gamma - N$ direction. Also given in **Table I** are the average specific heats C (defined in the Appendix) of the four compounds which show negligible variation, ~1.4%. None of these harmonic parameters, alone or combined, predict the first principles κ_l ordering of these systems: $\kappa_{La_3Cu_3P_4} < \kappa_{La_3Cu_3As_4} < \kappa_{La_3Cu_3Bi_4} < \kappa_{La_3Cu_3Sb_4}$. Thus, the anharmonic scattering of phonons in these systems must play a significant role in determining the κ_l behavior, whether by amount of scattering (phase space determined by conservation conditions) or by strength of each scattering process (anharmonic matrix elements - often measured by Grüneisen parameters).

TABLE I. Average atomic mass (M_{avg}), average Grüneisen parameter (γ), Debye temperature (Θ_D), room temperature specific heat (C) and calculated room temperature κ_l for each system. Definitions for γ, Θ_D and C can be found in the Appendix.

Compound	M_{avg} (amu)	γ	v_D (m/s)	Θ_D (K)	C (J/K. mol)	κ_l (W/m-K)
$La_3Cu_3P_4$	73.1	2.25	2700	298	488.2	1.31
$La_3Cu_3As_4$	90.7	1.81	2709	292	492.5	1.69
$La_3Cu_3Sb_4$	109.4	1.03	2791	287	493.7	3.35
$La_3Cu_3Bi_4$	144.3	1.15	2291	234	495.0	2.60

To gain further insights into the complicated combination of competing parameters that determine κ_l we first examine which modes provide the dominant conductivity. **Figure 1(b)** gives the accumulative lattice thermal conductivity (κ_{accum}) as a function of phonon frequency and scaled by the total κ_l for each system at 300 K. κ_{accum} gives the summed contribution from all modes below the specified frequency. For $La_3Cu_3P_4$, $La_3Cu_3As_4$ and $La_3Cu_3Bi_4$ phonons with frequency below ~3THz transport more than 80% of the heat, while for $La_3Cu_3Sb_4$ this is a bit less as some higher frequency modes within the optic spectrum are also contributing. Regardless, since the majority of the phonon transport is due to lower frequency acoustic phonons we restrict our subsequent discussions to the 0-3THz frequency window. Also, to further simplify discussions we compare only the lightest ($La_3Cu_3P_4$) and heaviest ($La_3Cu_3Bi_4$) systems in subsequent figures. Similar figures for $La_3Cu_3As_4$ and $La_3Cu_3Sb_4$ can be found in the Appendix.

Figures 2 (a) and **(b)** give the calculated low frequency phonon dispersions for $La_3Cu_3P_4$ and $La_3Cu_3Bi_4$, respectively. Phonon dispersions of $La_3Cu_3As_4$ and

$La_3Cu_3Sb_4$ compounds can be found in **Figure 6** of the Appendix. A general feature in both systems is significant mixing of the longitudinal acoustic (LA) branch with low-frequency optic branches. We note that optic phonons provide scattering channels for heat-carrying acoustic modes. Despite having very similar crystal structure there are striking differences in the phonon dispersions of these materials. Most noticeable are the "avoided crossings" of the LA branch of $La_3Cu_3P_4$ with the low-lying optic branches, behavior not seen in $La_3Cu_3Bi_4$. This is particularly noticeable along the Γ-N direction (see insets). As discussed in previous studies, avoided crossings are a manifestation of strong acoustic-optic coupling and have been argued to give lower κ_l in other systems [34-39]. Enhanced matrix elements have been correlated with these avoided crossing features in clathrates [39] and Fe_2Ge_3 [37]. Again, this anharmonicity can be characterized by mode Grüneisen parameters (γ_λ) [13,36,40]. As shown in **Figure 8(b)** of the Appendix $La_3Cu_3P_4$ and $La_3Cu_3As_4$ have larger γ_λ over the entire frequency range, and their values peak in the frequency range of the avoided crossings in these systems.

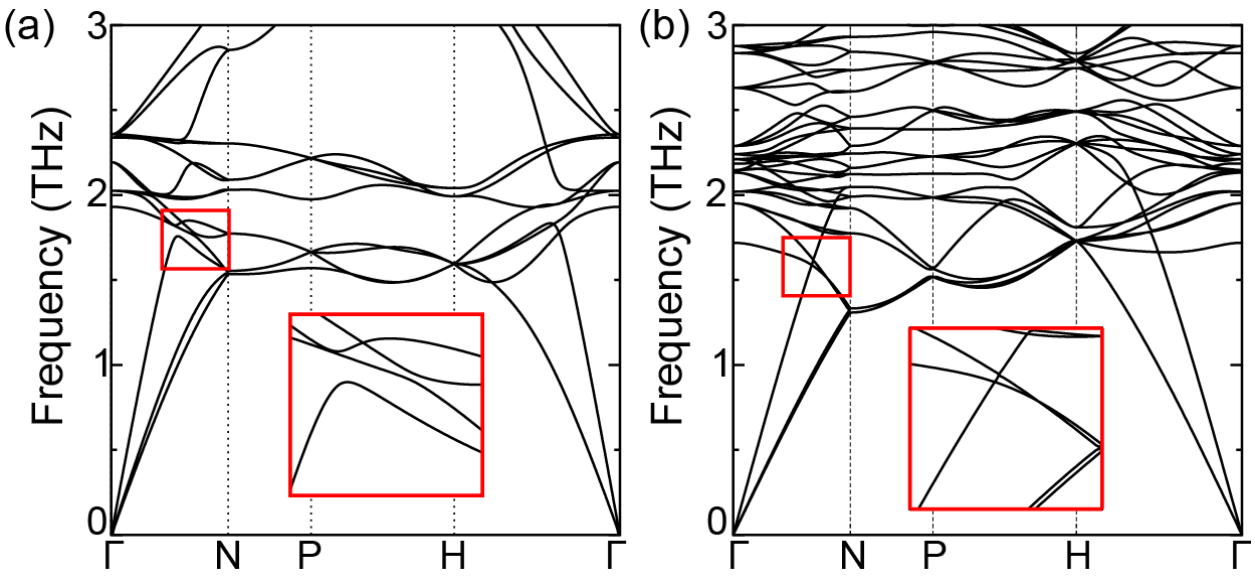

Figure 2. Calculated phonon dispersions for (a) $La_3Cu_3P_4$ and (b) $La_3Cu_3Bi_4$. The insets represent the enlargements of the red squares.

To elucidate the dispersion differences further, **Figures 3 (a) and (b)** give the partial phonon density of states (PDOS) of each atom type in $La_3Cu_3P_4$ and $La_3Cu_3Bi_4$, respectively. **Figure 7** in the Appendix compares the PDOS of $La_3Cu_3As_4$ and $La_3Cu_3Sb_4$. Typically, low frequency acoustic phonons are governed by the heaviest atoms; while the highest frequency optical phonons are governed by the lighter atoms. Indeed, we see that the heaviest atoms in $La_3Cu_3P_4$

(La atoms) and $La_3Cu_3Bi_4$ (Bi atoms) provide the dominant character to the acoustic modes in each system. From the point of view of the acoustic phonons $La_3Cu_3P_4$ and $La_3Cu_3Bi_4$ are very different systems as the La and Bi atoms sit at different lattice sites in the crystal structure. This may be a contributing factor in the varying LA optic crossing behaviors, and ultimately varying thermal conductivities.

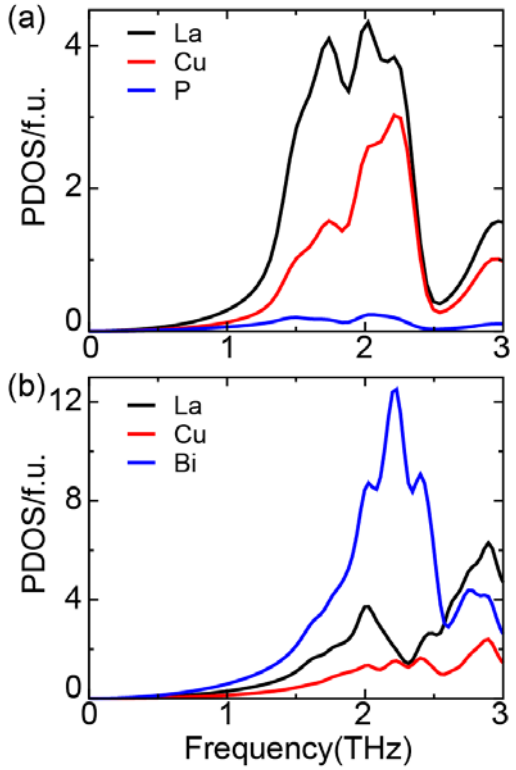

Figure 3. Calculated partial density of states (PDOS) for (a) $La_3Cu_3P_4$ and (b) $La_3Cu_3Bi_4$. Despite having similar crystal structure the PDOS of each system displays significantly different features.

The key missing feature not yet fully addressed is the anharmonicity, property (iv) discussed above. This governs the strength of phonon-phonon interactions through **Eqns. 2** and **3**, and ultimately determines the overall intrinsic thermal resistance - larger anharmonicity gives smaller phonon lifetimes. **Figure 4** shows the calculated intrinsic three-phonon scattering rates, $1/\tau_\lambda$, at 300 K for the heat-carrying acoustic modes of $La_3Cu_3P_4$ (pink diamonds) and $La_3Cu_3Bi_4$ (blue triangles). **Figure 8 (a)** of the Appendix gives the scattering rates for all systems. $La_3Cu_3P_4$ has the largest scattering rates for nearly all of the modes, especially at higher frequencies. The thermal resistance from these larger rates more than compensate the larger group velocities in $La_3Cu_3P_4$ thus giving lower overall κ_l than the other systems.

Often anharmonicity is measured by average (γ) or mode (γ_λ) Grüneisen

parameters (defined in the Appendix). **Table I** gives the calculated γ for each system, and follows the κ_l trend from first principles calculations. This is surprising as γ does not incorporate the complicated interplay of details in **Eqn. 2**: (i) anharmonic coupling strength, (ii) delta functions and (iii) phonon frequencies (directly and indirectly through the T-dependent Bose factors). In particular, a key missing feature is the microscopic structure of the "phase space" available for phonon-phonon scattering as limited by fundamental momentum and energy conservation conditions. Recently this scattering availability has emerged as a useful tool for understanding thermal transport in different classes of materials [41-46]. We note that phonon lifetimes and κ_l typically vary inversely with the available phase space [47].

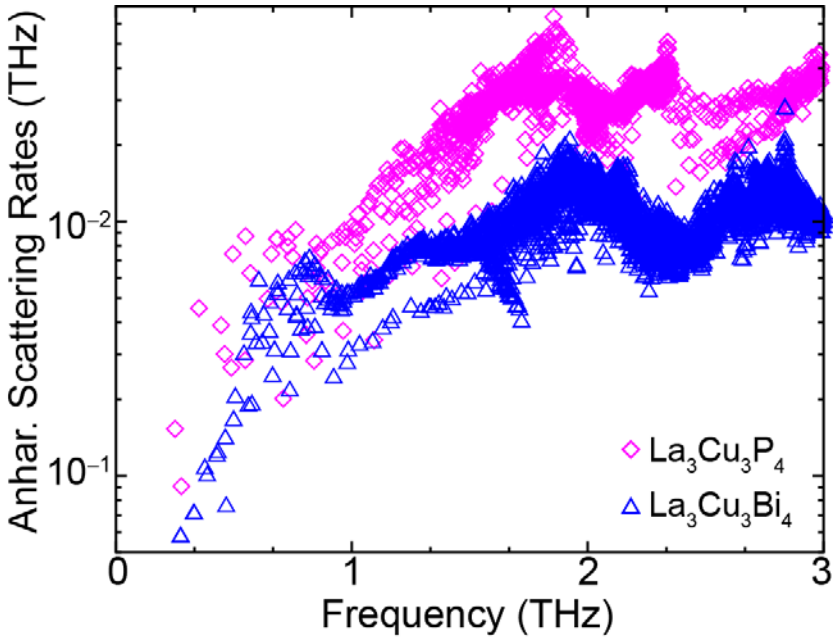

Figure 4. Calculated anharmonic scattering rates as a function of frequency for $La_3Cu_3P_4$ (pink diamonds) and (b) $La_3Cu_3Bi_4$ (blue triangles).

Figure 5(a) gives the weighted scattering phase space (number of processes allowed by conservation conditions) for $La_3Cu_3P_4$ and $La_3Cu_3Bi_4$. This is defined as the sum of possible three-phonon scatterings given conservation of energy and momentum weighted by the frequency factors in **Eq. 2**:

$$W_{\lambda}^{\pm} = \frac{1}{2N}\sum_{q,q'} \begin{Bmatrix} n_{\lambda'}^{0} - n_{\lambda''}^{0} \\ n_{\lambda'}^{0} + n_{\lambda''}^{0} + 1 \end{Bmatrix} \frac{\delta(\omega_{\lambda} \pm \omega_{\lambda'} - \omega_{\lambda''})}{\omega_{\lambda}\omega_{\lambda'}\omega_{\lambda''}} \qquad (4)$$

As the overall frequency scales of the $La_3Cu_3X_4$ systems are similar, particularly in the important lower frequency region, these frequency terms are likely not a significant factor driving phonon lifetime differences. Significantly more scattering is available for $La_3Cu_3Bi_4$, however, it has much smaller scattering rates (**Figure 4**) and larger κ_l. This is surprising as previous work has shown that the phase space is a robust indicator of κ_l trends among similar simple systems [24,35,39,41,44,47-50]. Thus, we find that all of the harmonic properties and tools for understanding κ_l (velocities, M_{avg}, Θ_D and scattering phase space) fail to describe the κ_l trend in the $La_3Cu_3X_4$ systems.

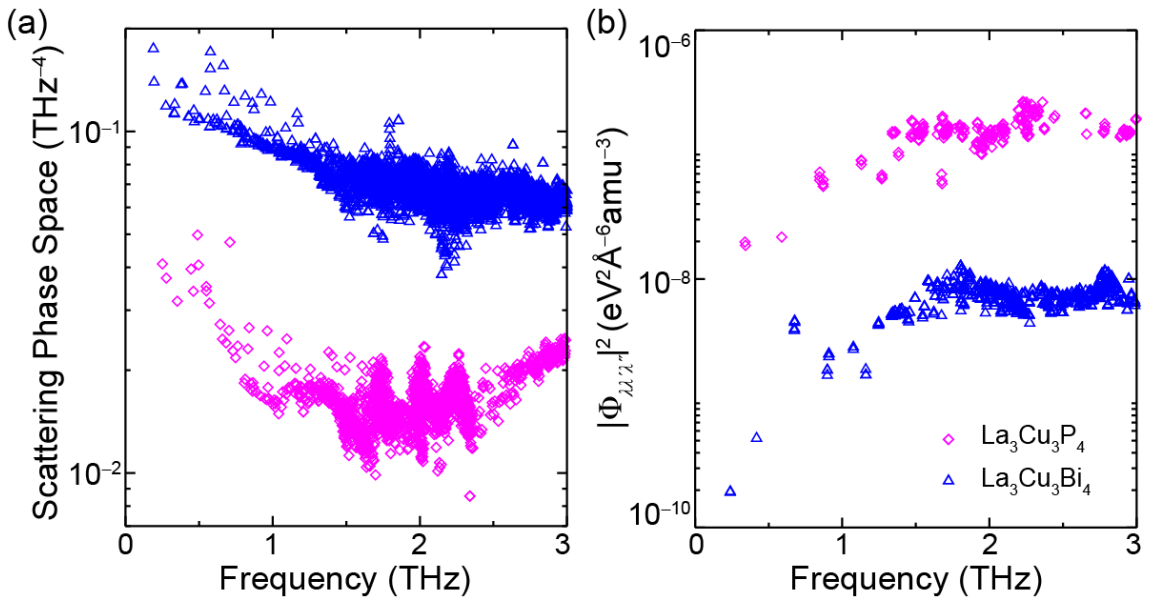

Figure 5: (a) Weighted phase space as a function of frequency for $La_3Cu_3P_4$ (pink diamonds) and $La_3Cu_3Bi_4$ (blue triangles). (b) Calculated average matrix elements $|\Phi_{\lambda\lambda'\lambda''}|^2$ from Eq. 3 as a function of frequency for $La_3Cu_3P_4$ and $La_3Cu_3Bi_4$, same symbols. Note that the $|\Phi_{\lambda\lambda'\lambda''}|^2$ for $La_3Cu_3P_4$ are much larger, thus overpowering the effects of it having a lower scattering phase space.

The only microscopic feature left to explore is the collection of individual transition matrix elements ($|\Phi_{\lambda\lambda'\lambda''}|^2$) appearing in **Eq. 2** and defined in Eq. 3. **Figure 5(b)** gives the average matrix elements calculated for each mode as a function of frequency for $La_3Cu_3P_4$ and $La_3Cu_3Bi_4$. These are averaged over thousands of transitions and can vary over many orders of magnitude dependent on the details of the interactions. As clearly shown in **Figure 5(b),** the matrix elements of $La_3Cu_3P_4$ are more than an order of magnitude stronger than those of $La_3Cu_3Bi_4$ over the entire frequency range. In fact, this difference is so large that the scattering rates in $La_3Cu_3P_4$ are significantly larger than in the other systems despite having the smallest available phase space: a smaller number of scattering

channels are providing more thermal resistance. Thus, $La_3Cu_3P_4$ has the smallest calculated κ_l despite harmonic features that would indicate that it should have the largest, corroborating the trend given by γ in **Table I**. We note that artificially adjusting the P atom mass to match that of Bi in the $La_3Cu_3P_4$ matrix elements accounts for only a small fraction of the differences of these terms with those of $La_3Cu_3Bi_4$. As seen in Eq. 3, $|\Phi_{\lambda\lambda'\lambda''}|^2$ terms are a complicated combination of masses, anharmonic IFCs, phase factors and eigenvectors. On comparing anharmonic IFCs we find that some $La_3Cu_3P_4$ terms are significantly larger than those in $La_3Cu_3Bi_4$, while others are significantly smaller. On average the $La_3Cu_3P_4$ anharmonic IFCs are ~16% larger, not enough to account for the matrix element differences shown in **Figure 5(b)**. To test this further we recalculated κ_l of $La_3Cu_3P_4$ but with the anharmonic IFCs of $La_3Cu_3Bi_4$. This results in only ~5% increase in κ_l, indicating that the magnitudes of the anharmonic IFCs are not driving the κ_l differences. However, the combination of $La_3Cu_3P_4$ harmonic IFCs with either anharmonic IFC set gives large scattering matrix elements. We again note that the heavy atoms that govern the heat-carrying acoustic vibrations sit at different symmetry sites on the crystal lattice. It is possible that this too plays a role in the varying magnitudes of the $|\Phi_{\lambda\lambda'\lambda''}|^2$ terms of these materials.

As shown in our recent work, these compounds are semiconducting with the bandgap in the range of 0.23 eV (for $La_3Cu_3Bi_4$) to 0.87 eV ($La_3Cu_3P_4$), which makes them interesting for potential thermoelectric applications [10]. All the compounds studied here exhibit large thermopower in the range of 180-250 μV/K, even at room temperature. The high thermopower together with calculated low thermal conductivity gives rise to a large figure of merit. In particular a Figure of merit of 1.5 was calculated theoretically for $La_3Cu_3P_4$ and $La_3Cu_3As_4$ under *p*-type doping. The detailed analysis of thermoelectric properties can be found in reference [10].

IV. SUMMARY AND CONCLUSIONS

To summarize, we have employed first principles phonon Boltzmann transport simulations to calculate vibrational and transport properties of complex unit cell $La_3Cu_3X_4$ systems (X=P, As, Sb, Bi). All systems have low κ_l (1.31W/m-K for $La_3Cu_3P_4$ and <4W/m-K for the other systems at room temperature) due to structural complexity and strong anharmonicity. These values are comparable to prominent thermoelectric materials such as PbTe and Bi_2Te_3. Despite having the lightest average atomic mass, $La_3Cu_3P_4$ has the lowest κ_l of the series. All harmonic properties, including average mass, specific heat, Debye temperature and phonon velocities, suggest that $La_3Cu_3P_4$ should have the highest κ_l. Even the

phase space for three-phonon scattering (an important tool for understanding phonon lifetimes) does not explain the thermal transport trends in these systems. We find that the anharmonic coupling elements from individual transition probabilities tend to be much stronger in $La_3Cu_3P_4$, giving strong thermal resistance despite having fewer scattering channels. This anharmonicity is also characterized by Grüneisen parameters and is correlated with observed avoided crossings of acoustic and optic branches in $La_3Cu_3P_4$ and $La_3Cu_3As_4$. The anharmonic coupling elements in combination with competing harmonic effects determine the overall κ_l trends in the $La_3Cu_3X_4$ systems. This work highlights the important role of anharmonicity and the complex interplay with harmonic vibrational features in determining thermal transport properties in complex systems important for thermoelectric and thermal barrier coating applications.

ACKNOWLDEDGMENTS

This work is supported by the U. S. Department of Energy, Office of Science, Office of Basic Energy Sciences, Materials Sciences and Engineering Division.

APPENDIX

The Debye temperature (Θ_D) can be determined by [51]:

$$\Theta_D = \frac{\hbar}{k_B} v_D \sqrt[3]{\frac{6\pi^2 N_0}{V}} \qquad (5)$$

where N_0 is the number of atoms, V is the crystal volume and v_D is the Debye velocity given by $v_{D^{-3}} = \frac{2}{3} v_{TA}^{-3} + \frac{1}{3} v_{LA}^{-3}$. v_{LA} and v_{TA} are the longitudinal and transverse sound velocities near the zone center along the $\Gamma - N$ direction.

The average Grüneisen parameter is defined as [52]:

$$\gamma = \sum_\lambda C_\lambda |\gamma_\lambda| / \sum_\lambda C_\lambda \qquad (6)$$

where γ_λ are mode Grüneisen parameters given by [53,54]:

$$\gamma_\lambda = -\frac{1}{6\omega_\lambda^2} \sum_{k,l'k',l''k''} \sum_{\alpha\beta\gamma} \Phi_{\alpha\beta\gamma}(0k, l'k', l''k'') \frac{e_{\alpha k}^{\lambda^*} e_{\beta k'}^{\lambda}}{\sqrt{m_k m_{k'}}} e_{i\boldsymbol{q}.\boldsymbol{R_l}} r_{l''k''\gamma} \quad (7)$$

where lk denotes the k^{th} atom in the l^{th} unit cell, $e_{\alpha k}^{\lambda}$ is the α^{th} component of the phonon eigenvector, $\boldsymbol{R_l}$, is the lattice vector of l^{th} unit cell, $r_{lk\alpha}$ is the α^{th} component of the vector locating the k^{th} atom in the l^{th} unit cell, and $\Phi_{\alpha\beta\gamma}(0k, l'k', l''k'')$ are the third order IFCs.

The volume normalized mode specific heat is computed as:

$$C_\lambda = \frac{\hbar\omega_\lambda (\partial n_\lambda^0 / \partial T)}{V} \qquad (8)$$

where n_λ^0 is the equilibrium Bose distribution, ω_λ is the phonon frequency in mode λ and V is the crystal volume.

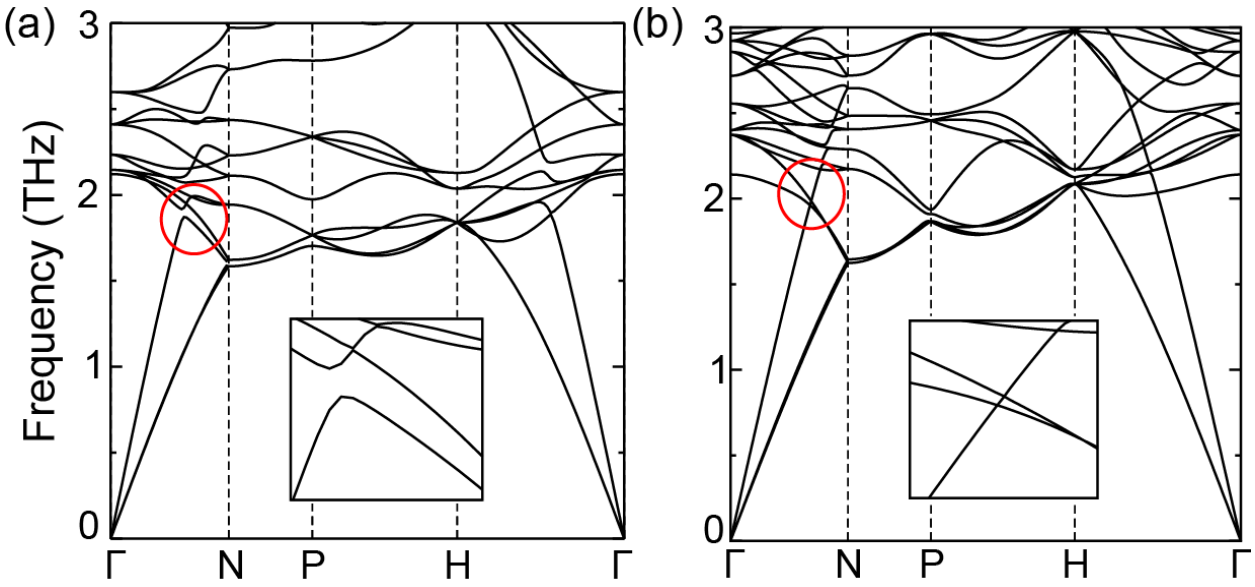

Figure 6: Calculated low frequency phonon dispersions for (a) $La_3Cu_3As_4$, and (b) $La_3Cu_3Sb_4$. The insets represent the enlargements of the red circles.

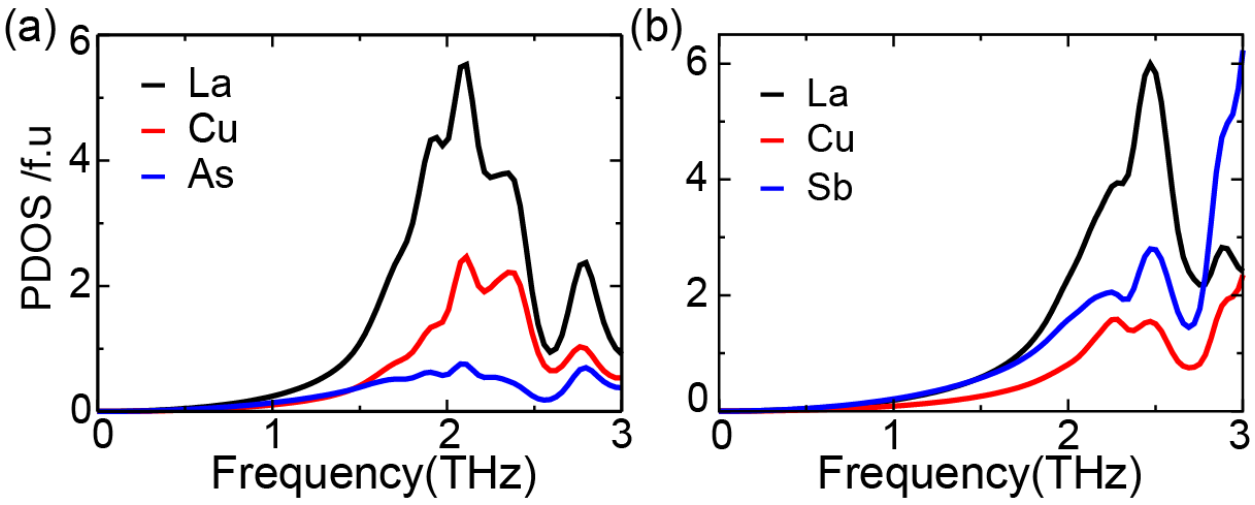

Figure 7: Calculated phonon density of states (PDOS) per formula unit for (a) $La_3Cu_3As_4$, and (b) $La_3Cu_3Sb_4$. Despite similar crystal structures, the PDOS have significantly different features.

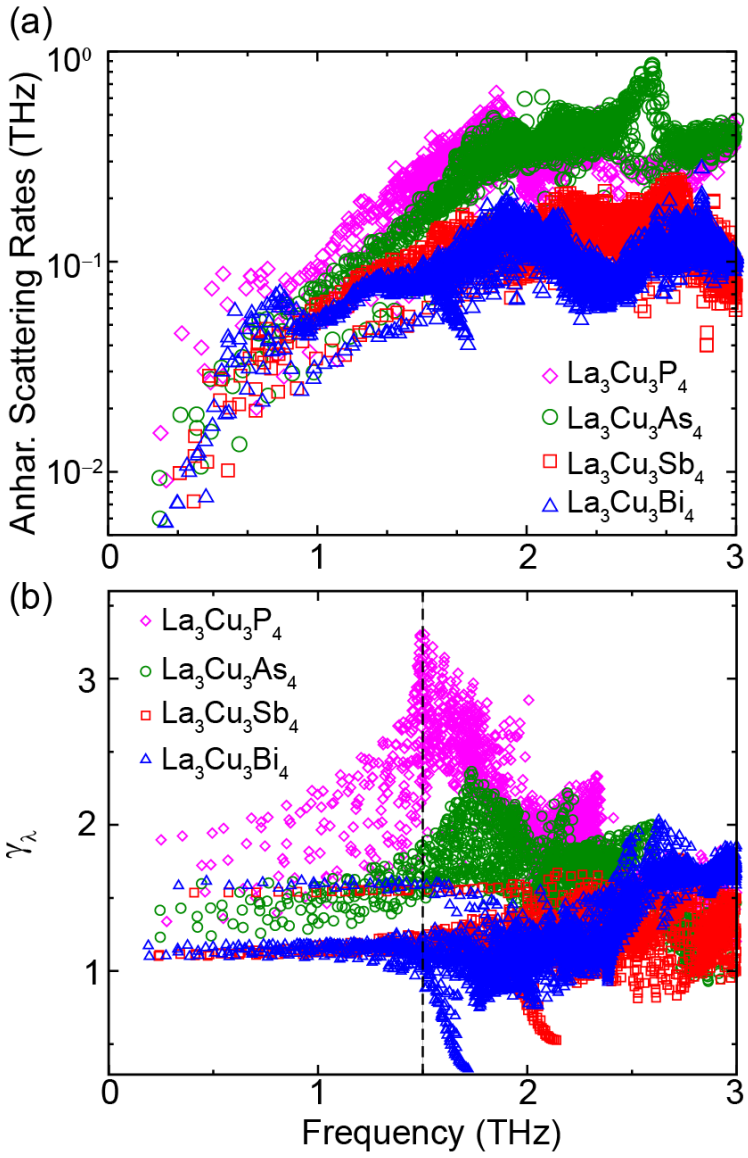

Figure 8: Calculated (a) anharmonic scattering rates and (b) mode Grüneisen parameters (γ_λ) as a function of frequency for $La_3Cu_3P_4$ (pink diamonds), $La_3Cu_3As_4$ (green circles), $La_3Cu_3Sb_4$ (red squares) and $La_3Cu_3Bi_4$ (blue triangles).

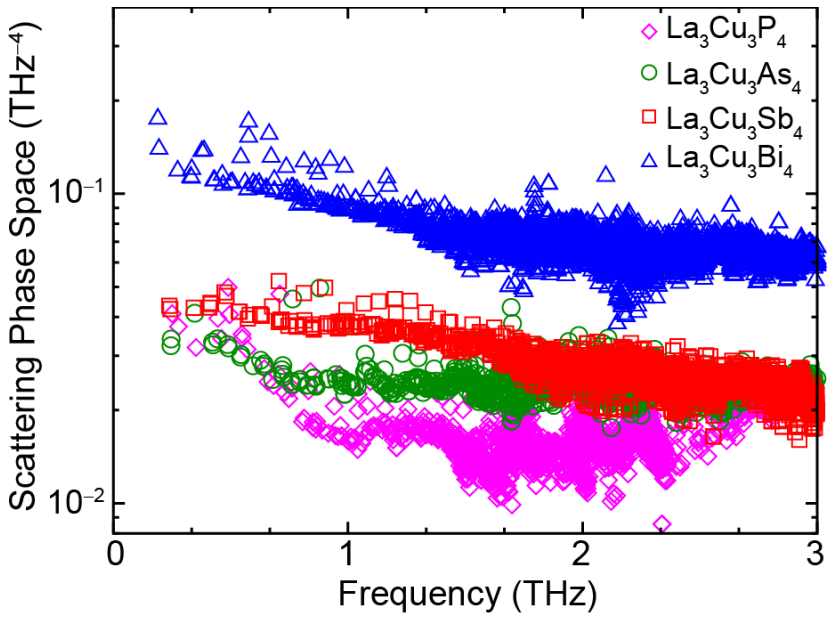

Figure 9: Calculated weighted phase space as a function of frequency for $La_3Cu_3P_4$ (pink diamonds), $La_3Cu_3As_4$ (green circles), $La_3Cu_3Sb_4$ (red squares), and $La_3Cu_3Bi_4$ (blue triangles).

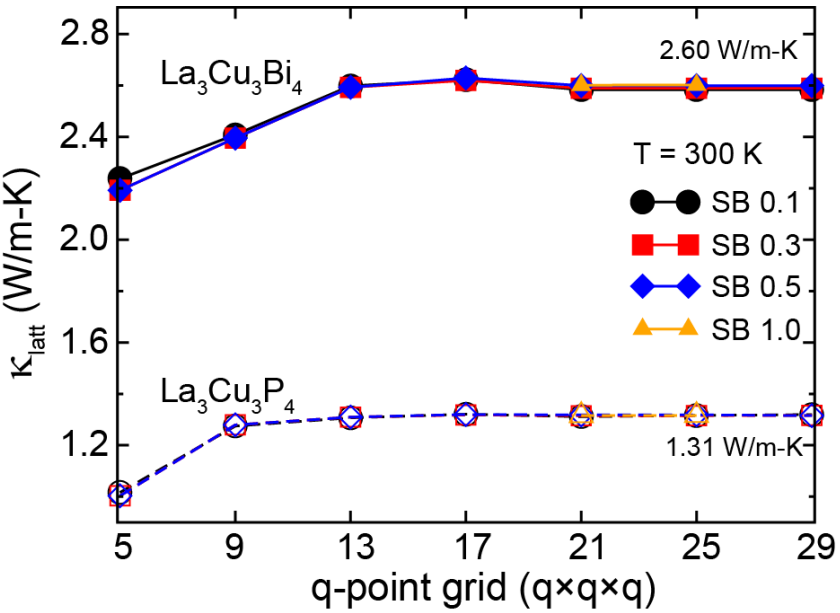

Figure 10: Convergence of room temperature κ_l for $La_3Cu_3Bi_4$ (solid lines) and $La_3Cu_3P_4$ (dotted lines) as a function of q-point grid at various Gaussian widths (shown by SB). κ_l is well converged for q-point integration grid of 25×25×25 and Gaussian width (SB) of 0.5.

[1] D. M. Rowe, *CRC handbook of thermoelectrics* (CRC press, Boca Raton, Florida, 1995).
[2] C. Wood, Rep. Prog. Phys. **51**, 459 (1988).
[3] G. Mahan and J. Sofo, Proc. Natl. Acad. Sci. U.S.A. **93**, 7436 (1996).
[4] G. A. Slack, J. Phys. Chem. Solids **34**, 321 (1973).
[5] G. A. Slack, Solid state physics **34**, 1 (1979).
[6] R. Skolozdra, P. Salamakha, A. Ganzyuk, and O. Bodak, Izvestiya Akademii Nauk-Rossijskaya Akademiya Nauk. Neorganicheskie Materialy **29**, 25 (1993).
[7] K. Fess, W. Kaefer, C. Thurner, K. Friemelt, C. Kloc, and E. Bucher, J. Appl. Phys. **83**, 2568 (1998).
[8] Y. M. Lu, F. Fan, C. M. Cai, S. X. Cao, and J. C. Zhang, J. Shanghai Univ. (English Edition) **12**, 486 (2008).
[9] Z. Hossain, S. Patil, R. Nagarajan, L. Gupta, R. Vijayaraghavan, and C. Godart, IEEE Trans. Magn. **30**, 4939 (1994).
[10] T. Pandey and D. S. Parker, *High potential thermoelectric figure of merit in ternary $La_3Cu_3X_4$ (X= P, As, Sb, and Bi) compounds, In preparation*.
[11] A. Jain and A. J. McGaughey, J. Appl. Phys. **116**, 073503 (2014).
[12] J. Ma, W. Li, and X. Luo, Appl. Phys. Lett. **108**, 082102 (2016).
[13] D. Morelli, V. Jovovic, and J. Heremans, Phys. Rev. Lett. **101**, 035901 (2008).
[14] S. Lee, K. Esfarjani, J. Mendoza, M. S. Dresselhaus, and G. Chen, Phys. Rev. B **89**, 085206 (2014).
[15] M. Omini and A. Sparavigna, Phys. Rev. B **53**, 9064 (1996).
[16] L. Lindsay, D. Broido, and T. Reinecke, Phys. Rev. B **87**, 165201 (2013).
[17] J. M. Ziman, *Electrons and phonons: the theory of transport phenomena in solids* (Oxford university press, 1960).
[18] A. Togo, F. Oba, and I. Tanaka, Phys. Rev. B **78**, 134106 (2008).
[19] A. Togo and I. Tanaka, Scr. Mater. **108**, 1 (2015).
[20] P. E. Blöchl, Phys. Rev. B **50**, 17953 (1994).
[21] G. Kresse and D. Joubert, Phys. Rev. B **59**, 1758 (1999).
[22] G. Kresse and J. Furthmüller, Comput. Mater. Sci. **6**, 15 (1996).
[23] J. P. Perdew, K. Burke, and M. Ernzerhof, Phys. Rev. Lett. **77**, 3865 (1996).
[24] W. Li, J. Carrete, N. A. Katcho, and N. Mingo, Comput. Phys. Commun. **185**, 1747 (2014).
[25] W. Li, N. Mingo, L. Lindsay, D. A. Broido, D. A. Stewart, and N. A. Katcho, Phys. Rev. B **85**, 195436 (2012).
[26] W. Li, L. Lindsay, D. Broido, D. A. Stewart, and N. Mingo, Phys. Rev. B **86**, 174307 (2012).
[27] *See Supplemental Material at http://link.aps.org/supplemental for crystal structure files and calculated harmonic and anharmonic IFCs.*
[28] S. I. Tamura, Phys. Rev. B **27**, 858 (1983).
[29] S. I. Tamura, Phys. Rev. B **30**, 849 (1984).
[30] C. Satterthwaite and R. Ure Jr, Phys. Rev. **108**, 1164 (1957).
[31] H. Goldsmid, Proceedings of the Physical Society. Section B **69**, 203 (1956).
[32] G. Leibfried, E. Schlömann, A. der Wissenschaften, and M.-p. Klasse, *Wärmeleitung in elektrisch isolierenden Kristallen, von Günther Leibfried und Ernst Schlömann* (Vandenhoeck und Ruprecht, 1954).
[33] D. T. Morelli and G. A. Slack, in *High thermal conductivity materials* (Springer, 2006), pp. 37.
[34] M. Christensen, A. B. Abrahamsen, N. B. Christensen, F. Juranyi, N. H. Andersen, K. Lefmann, J. Andreasson, C. R. Bahl, and B. B. Iversen, Nat. Mater. **7**, 811 (2008).
[35] W. Li and N. Mingo, Phys. Rev. B **91**, 144304 (2015).
[36] Y. Luo, J. Wang, Y. Li, and J. Wang, Sci. Rep. **6** (2016).

[37] W. Li, J. Carrete, G. K. Madsen, and N. Mingo, Phys. Rev. B **93**, 205203 (2016).
[38] O. Delaire *et al.*, Nat. Mater. **10**, 614 (2011).
[39] T. Tadano, Y. Gohda, and S. Tsuneyuki, Phys. Rev. Lett. **114**, 095501 (2015).
[40] L. D. Zhao, S. H. Lo, Y. Zhang, H. Sun, G. Tan, C. Uher, C. Wolverton, V. P. Dravid, and M. G. Kanatzidis, Nature **508**, 373 (2014).
[41] L. Lindsay, Nanosc. Microsc. Therm. **20**, 67 (2016).
[42] L. Lindsay, D. A. Broido, J. Carrete, N. Mingo, and T. L. Reinecke, Phys. Rev. B **91**, 121202 (2015).
[43] S. Lee, K. Esfarjani, T. Luo, J. Zhou, Z. Tian, and G. Chen, Nat. Commun. **5** (2014).
[44] T. Pandey and A. K. Singh, J. Mater. Chem. C **4**, 1979 (2016).
[45] G. Meisner, D. Morelli, S. Hu, J. Yang, and C. Uher, Phys. Rev. Lett. **80**, 3551 (1998).
[46] D. Broido, M. Malorny, G. Birner, N. Mingo, and D. Stewart, Appl. Phys. Lett. **91**, 231922 (2007).
[47] L. Lindsay and D. Broido, J. Phys. Condens. Matter **20**, 165209 (2008).
[48] A. Togo, L. Chaput, and I. Tanaka, Phys. Rev. B **91**, 094306 (2015).
[49] T. Pandey and A. K. Singh, Phys. Chem. Chem. Phys. **17**, 16917 (2015).
[50] T. Shibuya, J. M. Skelton, A. J. Jackson, K. Yasuoka, A. Togo, I. Tanaka, and A. Walsh, APL Mater. **4**, 104809 (2016).
[51] N. W. Ashcroft and N. D. Mermin, *Solid state physics* (Saunders College, Philadelphia, 1976).
[52] Y. Zhang, X. Ke, C. Chen, J. Yang, and P. Kent, Phys. Rev. B **80**, 024304 (2009).
[53] J. Fabian and P. B. Allen, Phys. Rev. Lett. **79**, 1885 (1997).
[54] D. Broido, A. Ward, and N. Mingo, Phys. Rev. B **72**, 014308 (2005).